Published in final edited form as:
Biochemistry. 2011 April 5; 50(13): 2456–2463. doi:10.1021/bi101803k.

Atomic structures suggest determinants of transmission barriers in mammalian prion disease

Marcin I. Apostol, **Jed J.W. Wiltzius**, **Michael R. Sawaya**, **Duilio Cascio**, and **David Eisenberg***
Howard Hughes Medical Institute, Department of Chemistry and Biochemistry, UCLA-DOE Institute, UCLA, 611 Charles Young Drive East, Los Angeles CA 90095-1570

Abstract

Prion represents a unique class of pathogens devoid of nucleic acid. The deadly diseases transmitted by it between members of one species and, in certain instances to members of other species, present a public health concern. Transmissibility and the barriers to transmission between species have been suggested to arise from the degree to which a pathological protein conformation from an individual of one species can seed a pathological conformation in another species. However, this hypothesis has never been illustrated at an atomic level. Here we present three X-ray atomic structures of the same segment from human, mouse, and hamster PrP, which is critical for forming amyloid and confers species specificity in PrP seeding experiments. The structures reveal that different sequences encode different steric zippers and suggest that the degree of dissimilarity of these zipper structures gives rise to transmission barriers in prion disease, such as those that protect humans from acquiring bovine spongiform encephalopathy (BSE) and chronic wasting disease (CWD).

Keywords

X-ray crystallography; steric zipper; prion; transmission barrier; species barrier

Prion diseases are also known as transmissible spongiform encephalopathies (TSE) underscoring one of their most intriguing properties: their infectivity without DNA or RNA. Transmission of prion disease has been observed between individuals of the same species, such as with the disease Kuru in humans, Scrapie in sheep and goats, and chronic wasting disease (CWD) in deer and elk. However, in the 1990's the ability of prion disease to cross species boundaries created a world-wide public health concern during the highly publicized scare of "mad cow disease," when an outbreak of bovine spongiform encephalopathy (BSE) apparently spread through the food chain to manifest itself in humans as variant Creutzfeldt-Jakob Disease (vCJD) (1,2). This outbreak triggered scientific questions about the existence of "species barriers" to prion transmission. Interestingly, both domestic cats and captive wild cats who were fed with the tainted beef also succumbed to the disease, but other animals such as dogs did not (3,4). Species barriers also exist which protect humans from the transmission of Scrapie from sheep and goats, and which protect humans and cattle from the transmission of CWD from cervids (5–7).

Prion replication is independent of nucleic acids representing a novel paradigm in biology known as 'protein-only' inheritance, hence the molecular mechanisms of its infectious nature and species barriers have not yet been fully understood. It is known that prion

*To whom correspondence should be addressed to: david@mbi.ucla.edu; phone, (310)825-3754; fax, (310)206-3914.

diseases are transmitted through a self-propagating aggregated isoform (PrP^{Sc}) of the prion protein which recruits endogenous monomeric prion protein (PrP^{C}) into the PrP^{Sc} form (8). Aggregated PrP^{Sc} deposits as extracellular plaques predominantly in brain tissues of humans and animals affected by disease. Although in isolation pathogenic PrP^{Sc} has been found to have characteristics of amyloid (9–11), in contrast to other similar neurodegenerative diseases such as Alzheimers, Parkinsons's and Huntingon in which proteins deposit into plaques composed of amyloid fibers, *in vivo* plaques of PrP^{Sc} do not always resemble amyloid fibers(12). Nonetheless, the properties of prion transmission bear a striking mechanistic resemblance to the seeded polymerization of amyloid fibers from a pool of unpolymerized protein (13–15). Although there is not yet any universal agreement on the molecular basis of prion infectivity, amyloid has been used as a model to explore the mechanism of species barriers in its transmission.

The sequence of PrP is extremely similar among mammals, and single amino acid differences found between species have been shown experimentally to give rise to the barriers (16–18). However, such simple explanations are complicated by the additional observation that different "strains" of prion from the same species do not always share the same barriers. For example, laboratory experiments have shown that mice develop prion disease when inoculated with vCJD, but are not susceptible if inoculated with the sporadic form of CJD (sCJD), both of which arise from PrP^{Sc} with the same primary sequence (19,20). Prion strains have been characterized as different "conformational" states of PrP that give rise to distinct disease incubation times and neuropathology, such as those seen between vCJD and sCJD (21). In previous work we have shown that strains of amyloid may be encoded by distinct three-dimensional structures with alternative packing arrangements of beta-sheets formed from segments of amyloidogenic proteins (22). It has been proposed by Clarke and Collinge that species barriers and strains are intimately linked by the idea that a barrier exists when one strain cannot be propagated by the monomer of another due to the inability of the recipient's PrP sequence to adopt that same structure (23). The term "transmission barrier" has been suggested by Collinge instead of "species barrier," in that a structural explanation of the phenomenon can reconcile both species and strain dependent barriers to prion infection (2,23). However, currently there are no atomic structures of PrP^{Sc} known with which this hypothesis can be illustrated.

Here we explore the structural determinants of an experimentally verified strain-dependent species barrier observed in recombinant mammalian PrP. We determined the atomic structures of segments of human, mouse, and hamster from an identical region encompassing residues 138–144 of PrP (using human numbering). This region was shown to be critical for amyloid formation in a C-terminally truncated human prion (PrP23-144) that is the major component of amyloid plaques in individuals with GSS (Gerstmann-Sträussler-Scheinker syndrome) who carry a mutation resulting in a stop codon at position 145 (24). Studies by Vanik *et al.* on similarly truncated prions from mouse and Syrian hamster found not only distinct structural morphologies of amyloid fibrils formed from the different species, but also corresponding cross-seeding behavior dictated by these structural differences (25). The basis of these differences was narrowed down to sequence variation in amino acid residue positions 138 and 139 which can be either methionine or isoleucine, depending on the species. By substitution of only these two species specific amino acids, Jones *et al.* showed that the human and mouse sequences form similar strains which can mutually seed the formation of amyloid (26). However, the hamster sequence forms a strain different from the other two that cannot be seeded by either preformed human or mouse amyloid, but in turn can seed the mouse prion (Table 1). Interestingly the seeded mouse protein took on the characteristics of the hamster strain.

Although the transmission barrier described above reflects a phenomenon found *in vitro*, it is suggestive of the mechanisms that can exist *in vivo*. Here we discuss this transmission barrier in terms of other segment structures we have determined that contain parts of the prion sequence that have been implicated in transmission barriers for BSE and CWD to humans and other species.

MATERIALS AND METHODS

Crystallization

All peptides were purchased in 30 or 50mg batches with a 99% purity from CS BIO Inc. (Menlo Park, CA). Initial crystallization conditions were found using the Index Screen from Hampton Research (Aliso Viejo, CA) and further optimized using the hanging drop method. Crystals of Ham138–143 were grown in 1.2 M Ammonium sulfate and 200 mM Bis-Tris pH 7.5 with the peptide dissolved in 15% acetonitrile, 15 mM Bis-Tris at a concentration of 40mg/ml. Crystals of Hum138–143 were grown in 100mM Tris pH 7.4 and 25% 2-methyl-2,4-pentanediol (MPD) with the peptide initially dissolved in 15% acetonitile, 15 mM Bis-Tris at a concentration of 40 mg/ml. Mus137–142 was dissolved in water at a concentration of 30 mg/ml and crystallized from 100 mM HEPES pH 7.5. Mus137–143 was dissolved in water at a concentration of 35 mg/ml and crystallized in 100mM HEPES ph 7.0 and 10% PEG 1200.

Data collection

In the case of Hum138–143, Mus137–142 and Mus137–143, crystals grew as thin needles 5–10 micrometers in width and hundreds of micrometers in length. Because of the small size of the crystals we used micro-diffraction beamlines ID13 at the European Synchrotron Radiation Facility (ESRF) located in Grenoble, France and X06SA at the Swiss Light Source (SLS) located in Villigen, Switzerland. These crystals were mounted directly onto the ends of pulled glass capillaries. Because of the tight packing between segments in the crystals, no cryoprotectant was needed in the crystals; however the crystals were cooled to −180°C during data collection. The Ham138–143 crystals grew as thin plate-like crystals and did not require the use of a small diameter beam. The crystals were mounted in loops standard for protein crystallography from Hampton Research using glycerol as a cryoprotectant. Data were collected at our home-source rotating copper anode generator at UCLA (Rigaku-FRD) using a Rigaku RAXIS-4++ image plate detector. In all cases data were collected using 5° wedges.

Data Processing

Indexing of diffraction images were performed using the programs DENZO (27) or XDS (28). Scaling of data was performed using the program SCALEPACK (27). The merged scaled data was imported into the CCP4 format with programs from the CCP4 program suite organized under the “CCP4i” interface (29).

Structure determination and refinement

Phases were determined using the molecular replacement method with the program PHASER (30) initially using an idealized polyalanine beta-strand. The program COOT (31) was used for model building along with rounds of refinement with the program REFMAC (32). Data statistics can be found in Table 2.

Illustration of structures

Protein structures were illustrated using the program PyMol (33).

Accession Codes

Structures have been deposited in the Protein Data Bank as 3NVE for Ham138–143, 3NVF for Hum138–143, 3NVG for Mus137–142, and 3NVH for Mus137–143.

RESULTS

We crystallized segments of human, mouse, and hamster sequences corresponding to residues 138–143 (mouse numbering: Mus137–142) for six-residue segments, and 138–144 (Mus137–143) for seven residue segments. Both six and seven-residue segments contain the species specific residues that give rise to strain differences. Structure determination was possible from crystals of all three six-residue segments, and in addition, the mouse seven-residue segment.

The human (Hum138–143) and mouse segments (Mus137–142 and Mus137–143) crystallized in the same space group with very similar unit cell dimensions (Table 2). Segments from both species formed Class 1 parallel steric zippers; meaning that within each of the two beta-sheets, individual beta-strands run in the same direction and the sheets pack together in a parallel, face-to-face arrangement (Figure 1a,b,d, and e) (34). Removed from the beta-sheets, the individual strands of the six- and seven-residue mouse segments as well as the six-residue human segment can be directly superimposed on each other illustrating nearly identical structural characteristics with very low root mean square deviations (Figure 1g, Table 3). The flexibility of the glycine residue at position 142 (human numbering) contributes a kink to the beta-sheet seen in the human and mouse structures.

In contrast, the Syrian hamster segment (Ham138–143) forms a class 6 anti-parallel steric zipper where adjacent beta-strands run in opposite directions within beta-sheets. A translation relates one sheet in the interface to the other, packing in a face-to-back orientation (Fig. 1c). The anti-parallel arrangement results in a stacking of side-chains Met138/Gly142, Met139/Phe143, and His140/His140 along the main chain hydrogen bonding direction of the beta-sheets (Fig. 1f). Unusually for anti-parallel steric zippers which typically have identical faces, each face of the beta-sheet of Ham138–143 is not equivalent. This results in all Met138 residues protruding to one side of the sheet, while Met139 protrudes to the other. However, due to the face-to-back packing, both Met138 and Met139 which were found to be critical for the transmission barrier are within the interface. Unlike the human and mouse structures, Gly142 does not contribute a kink in the beta-sheet; the strands are straight and extended in the hamster segment. These structural differences appear to be encoded by the variation in sequences of the peptides rather than influenced by variation in crystallization condition. If the latter had been the more critical factor, crystal seeding experiments would have been successful in producing isomorphous crystals under identical conditions. Such was not the case, as discussed below.

The phenomenon of seeding is well known and widely used in the field of protein crystallography. We attempted to reproduce the species specific seeding effects seen on amyloid fibers of PrP23-144 in our segment crystals reflective of amyloid structure. The crystal structure of the hamster segment is distinct from human and mouse and we were interested to determine if we could induce the monomeric human and mouse segments to adopt the structural characteristics of the hamster segment by using preformed crystals as seeds. However, seeding human and mouse monomers with hamster segment crystals never yielded alternative crystal forms when checked with X-ray diffraction. Possible reasons for the failure of this experiment are discussed below. Seeding of human monomer with preformed mouse crystals and vice-versa did show seeding, however crystal forms were identical when probed with X-ray diffraction, as would be expected from the nearly identical structures.

DISCUSSION

Whereas the structure of a short segment from a globular protein would be uninformative about the structure or action of the entire protein, in the amyloid state the spine of the fibril is formed from stacks of identical, short sequence segments from identical molecules. Thus the crystal structure of such a steric zipper reveals the structure of the spine of the fibril. In the amyloid form of PrP, there appear to be several potential steric zipper spines, one of them—the 138–144 segment.

The structures of segment 138–144 suggest a molecular mechanism underlying the phenomenon of transmission barriers. The conformation of the human and mouse segments within our crystal structures are nearly identical; both form parallel steric zippers with a characteristic kink within the beta-strands at Gly142. However, the hamster segment crystallized in a different conformation, as an anti-parallel steric zipper. Drawing an analogy between peptide conformation and “strain”, the human and mouse structures could be considered identical “strains” despite sequence variation, while the hamster segment could be considered an alternate “strain”. The pattern of similarities and differences among our human, mouse, and hamster crystal structures are related to the pattern of fibril morphologies and seeding propensities among PrP23-144 from the same three species (Table 1) observed by Vanik *et al.* and Jones *et al.* (25,26). That is, the pair of peptides showing the most similar conformations or “strains” (i.e. mouse and human) originated from the same pair of species in which PrP23-144 fibril seeding is productive in either direction ([Mus]-Hum or [Hum]-Mus). In contrast, the peptide showing the least similarities to the other two (i.e. hamster) originated from the only species in which PrP23-144 cannot be coaxed into fibrils by seeds of the remaining two.

This observed correlation between peptide structure and fibril seeding propensity is consistent with the idea that fibril seeding propensity is guided by the compatibility of the protein monomer with the conformation of the template seed. The bent conformation is energetically more favorable for the mouse and human peptides, and the extended conformation is energetically more favorable for the hamster peptide. In figure 2, we illustrate their compatibilities as structural fits of the preferred structure of segments 138–143 onto templates of preformed seed of another species’ segment. Table 3 reports a quantitative measure for structural fit. The relative qualities of these fits explain five of the six resultant strain dependent seeding phenomenon, or transmission barriers, observed by Jones et. al (26). The one enigmatic case, the ability of the hamster strain to seed the growth of mouse fibrils, is contradicted by the dissimilarity of the two species’ preferred conformations. The mouse and hamster segments both share a methionine at position 138 suggesting that this residue may be critical in its ability to adapt both strain types, although we were not able to confirm this with crystal seeding experiments. The Met138 residue is indeed found at the interface of the beta-sheets of the hamster segment’s steric zipper but is irrelevant to the interfaces found within the mouse structures (Figure 1). In the context of the full-length prion protein, it is uncertain whether the cross-β spines of the three peptide segments presented here are maintained, or adopt a different symmetry. It is remarkable, however, that the pattern of structural similarities and differences among these peptides mirrors the pattern of transmission barriers between species and results obtained from seeding experiments conducted on much larger fragments of the prion protein. These correlations suggest that the peptides are on some level representative of the spines present in PrP, and therefore useful as a starting atomic-level mechanism for transmission barriers.

By similar arguments, the transmission barrier between cows and humans could be explained by the incompatibility of atomic structures of another prion segment. We have previously described the structures of polymorphs of human prion segment 127–132

(GY**M**LGS and GY**V**LGS) (35); like segment 138–144, this segment has also been implicated in transmission barriers *in vivo*. Specifically, the human polymorphism at codon 129 has been shown to be critical in creating a transmission barrier of BSE to humans. Cows do not share such a polymorphism, hence bovine PrP only carries a methionine residue at position 129. The polymorphism in humans produces a valine or methionine at this same position. However, BSE has only been found to be infectious to individuals who have the methionine (36,37). We have shown that the segment 127–132 with M129 or V129 have incompatible steric zipper interfaces (35). This implies that bovine PrP^{Sc} also utilizes the same segment for assembly and suggests why humans that are predominantly homozygous at the M129 locus are the only individuals prone to BSE (36,37).

In the related disease, CWD, yet a third segment of prion (170–175 using human numbering) has been implicated in transmission barriers between cervids and other mammals. Again, incompatible steric zipper interfaces could explain the barrier. Cervids such as elk and deer can readily develop CWD which is extremely contagious among animals in close contact (38–40). The cervid family share Asn and Thr at positions 170 and 174 (**N**NQN**T**F) (positions 173 and 178 using elk numbering). Humans, mice, and cows all share a different sequence of segment 170–175 (**S**NQN**N**F)(using human numbering, Figure 3a) along with resistance to CWD (5–7,41,42). The cervid specific amino acids were found to limit the dynamics of a loop in the monomeric cervid PrP^{C} solution structure and when substituted into the sequence of mouse PrP the “cervidized” transgenic mice developed a spontaneous prion disease which cannot be passaged directly to wild-type mice (43,44). Furthermore, the “cervidized” transgenic mice become susceptible to inoculation by prion strains, such as CWD, which wild-type mice are normally protected from by a transmission barrier, and conversely become protected by a transmission barrier from prion strains which wild-type mice are susceptible to (45). A comparison of the two previously published segments 173–178 (sequence NNQNTF) of the cervid PrP and 170–175 (SNQNNF) of human PrP show that despite slight changes in sequence, the two have distinct steric zipper structures suggestive of the reasons for the transmission barrier (Figure 3b–d) (22,34). Of note is that one face of the beta sheets from the human and elk segments has the same characteristic residues xNxNxF (figure 3a) while the other face contains amino acid substitutions characteristic of the differences between the cervid family and other mammals. The homotypic steric zipper interfaces seen between the xNxNxF faces of the elk segment are not recapitulated within the human segment. The human segment has a smaller sheet-to-sheet interface than either of the two interfaces seen in the elk segment and suggests that the N170 and T174 residues may facilitate the assembly of elk prion into a stronger and more prototypical steric zipper similar to that seen in the yeast prion segment NNQQNY (46). The importance of the segment 170–175 in transmission barriers is further supported by the fact that rabbits, whose prion protein sequence is unique from other mammals because of a serine residue at position 174, are resistant to infection by TSE from other species (18,47).

Our results indicate that small changes in amino acid residues, even conservative changes such as isoleucine to methionine, can profoundly influence steric zipper structures. Factors that influence the assembly of steric zippers include not only how side chains pack at the interface of beta-sheets but also how they stack in beta-sheets. The crystal structures of human, mouse, and hamster PrP segments 138–143 suggest an atomic mechanism to explain how the sequence of prions can influence amyloid structure and how that in turn can influence strain propagation in a pool of monomeric prion with a different sequence. The ability to propagate strains formed from one species in another with a distinct PrP sequence is the key to the phenomenon of transmission barriers. The results we present here suggest structural compatibility as a molecular mechanism for how specific amino acid changes can give rise to transmission barriers by hindering amyloidogenic segments from adopting similar steric zipper structures.

Acknowledgments

We thank the staff of the European Synchrotron Radiation Facility beamline ID-13 and Swiss Light Source beamline X-06-SA for support and assistance with data collection. We are particularly indebted to Ehmke Pohl for spending time and resources in screening crystals and collecting diffraction data. We thank Devdoot Majumdar and Matthew Graf for their help with the experimental aspects of this manuscript, Natalie Anderson for critical reading of the manuscript, and NSF, NIH, and HHMI for support.

This study was supported by grants from the NIH, NSF, DOD, and HHMI. M.I.A. thanks the support of the Ruth L. Kirschstein National Research Service Award GM007185 and the UCLA Dissertation Year Fellowship.

Abbreviations

PrP	prion protein
PrP^C	cellular prion protein
PrP^{Sc}	pathogenic scrapie prion
Hum	human
Mus	mouse
Ham	hamster
TSE	transmissible spongiform encephalopathy
BSE	bovine spongiform encephalopathy
CJD	Creutzfeldt-Jakob disease
GSS	Gerstmann-Sträussler-Scheinker syndrome
r.m.s.d.	root mean square deviation

REFERENCES

1. Hilton DA. Pathogenesis and prevalence of variant Creutzfeldt-Jakob disease. J. Pathol. 2006; 208:134–141. [PubMed: 16362983]
2. Collinge J. Variant Creutzfeldt-Jakob disease. The Lancet. 1999; 354:317–323.
3. Aldhous P. BSE: spongiform encephalopathy found in cat. Nature. 1990; 345:194. [PubMed: 2333092]
4. Kirkwood JK, Cunningham AA. Epidemiological observations on spongiform encephalopathies in captive wild animals in the British Isles. Vet. Rec. 1994; 135:296–303. [PubMed: 7817514]
5. Sigurdson CJ, Aguzzi A. Chronic wasting disease. Biochim. Biophys. Acta. 2007; 1772:610–618. [PubMed: 17223321]
6. Belay ED, Maddox RA, Williams ES, Miller MW, Gambetti P, Schonberger LB. Chronic wasting disease and potential transmission to humans. Emerging Infect. Dis. 2004; 10:977–984. [PubMed: 15207045]
7. Hamir AN, Kunkle RA, Cutlip RC, Miller JM, O'Rourke KI, Williams ES, Miller MW, Stack MJ, Chaplin MJ, Richt JA. Experimental transmission of chronic wasting disease agent from mule deer to cattle by the intracerebral route. J. Vet. Diagn. Invest. 2005; 17:276–281. [PubMed: 15945388]
8. Prusiner SB. Inherited prion diseases. Proc. Natl. Acad. Sci. U.S.A. 1994; 91:4611–4614. [PubMed: 8197105]
9. Prusiner SB, McKinley MP, Bowman KA, Bolton DC, Bendheim PE, Groth DF, Glenner GG. Scrapie prions aggregate to form amyloid-like birefringent rods. Cell. 1983; 35:349–358. [PubMed: 6418385]
10. Nguyen JT, Inouye H, Baldwin MA, Fletterick RJ, Cohen FE, Prusiner SB, Kirschner DA. X-ray Diffraction of Scrapie Prion Rods and PrP Peptides. Journal of Molecular Biology. 1995; 252:412–422. [PubMed: 7563061]

11. Wille H, Bian W, McDonald M, Kendall A, Colby DW, Bloch L, Ollesch J, Borovinskiy AL, Cohen FE, Prusiner SB, Stubbs G. Natural and synthetic prion structure from X-ray fiber diffraction. Proc. Natl. Acad. Sci. U.S.A. 2009; 106:16990–16995. [PubMed: 19805070]
12. DeArmond SJ. Discovering the mechanisms of neurodegeneration in prion diseases. Neurochem. Res. 2004; 29:1979–1998. [PubMed: 15662833]
13. Jarrett JT, Lansbury PT. Seeding "one-dimensional crystallization" of amyloid: a pathogenic mechanism in Alzheimer's disease and scrapie? Cell. 1993; 73:1055–1058. [PubMed: 8513491]
14. Hall D, Edskes H. Silent prions lying in wait: a two-hit model of prion/amyloid formation and infection. J. Mol. Biol. 2004; 336:775–786. [PubMed: 15095987]
15. Griffith JS. Self-replication and scrapie. Nature. 1967; 215:1043–1044. [PubMed: 4964084]
16. Scott M, Groth D, Foster D, Torchia M, Yang SL, DeArmond SJ, Prusiner SB. Propagation of prions with artificial properties in transgenic mice expressing chimeric PrP genes. Cell. 1993; 73:979–988. [PubMed: 8098995]
17. Prusiner SB, Scott M, Foster D, Pan K, Groth D, Mirenda C, Torchia M, Yang S, Serban D, Carlson GA, Hoppe PC, Westaway D, DeArmond SJ. Transgenetic studies implicate interactions between homologous PrP isoforms in scrapie prion replication. Cell. 1990; 63:673–686. [PubMed: 1977523]
18. Vorberg I, Groschup MH, Pfaff E, Priola SA. Multiple amino acid residues within the rabbit prion protein inhibit formation of its abnormal isoform. J. Virol. 2003; 77:2003–2009. [PubMed: 12525634]
19. Hill AF, Desbruslais M, Joiner S, Sidle KC, Gowland I, Collinge J, Doey LJ, Lantos P. The same prion strain causes vCJD and BSE. Nature. 1997; 389:448–450. 526. [PubMed: 9333232]
20. Collinge J, Palmer MS, Sidle KC, Hill AF, Gowland I, Meads J, Asante E, Bradley R, Doey LJ, Lantos PL. Unaltered susceptibility to BSE in transgenic mice expressing human prion protein. Nature. 1995; 378:779–783. [PubMed: 8524411]
21. Collinge J, Sidle KC, Meads J, Ironside J, Hill AF. Molecular analysis of prion strain variation and the aetiology of 'new variant' CJD. Nature. 1996; 383:685–690. [PubMed: 8878476]
22. Wiltzius JJW, Landau M, Nelson R, Sawaya MR, Apostol MI, Goldschmidt L, Soriaga AB, Cascio D, Rajashankar K, Eisenberg D. Molecular mechanisms for protein-encoded inheritance. Nat Struct Mol Biol. 2009; 16:973–978. [PubMed: 19684598]
23. Collinge J, Clarke AR. A General Model of Prion Strains and Their Pathogenicity. Science. 2007; 318:930–936. [PubMed: 17991853]
24. Kundu B, Maiti NR, Jones EM, Surewicz KA, Vanik DL, Surewicz WK. Nucleation-dependent conformational conversion of the Y145Stop variant of human prion protein: Structural clues for prion propagation. Proceedings of the National Academy of Sciences of the United States of America. 2003; 100:12069–12074. [PubMed: 14519851]
25. Vanik DL, Surewicz KA, Surewicz WK. Molecular basis of barriers for interspecies transmissibility of mammalian prions. Mol. Cell. 2004; 14:139–145. [PubMed: 15068810]
26. Jones EM, Surewicz WK. Fibril conformation as the basis of species- and strain-dependent seeding specificity of mammalian prion amyloids. Cell. 2005; 121:63–72. [PubMed: 15820679]
27. Otwinowski, Z.; Minor, W. Methods in Enzymology. Academic Press; 1997. Processing of X-ray Diffraction Data Collected in Oscillation Mode; p. 307-326.
28. Kabsch W. Automatic processing of rotation diffraction data from crystals of initially unknown symmetry and cell constants. J Appl Crystallogr. 1993; 26:795–800.
29. Collaborative Computational Project, Number 4. The CCP4 suite: programs for protein crystallography. Acta Crystallogr D Biol Crystallogr. 1994; 50:760–763. [PubMed: 15299374]
30. McCoy AJ, Grosse-Kunstleve RW, Adams PD, Winn MD, Storoni LC, Read RJ. Phaser crsytallographic software. J Appl Crystallogr. 2007; 40:658–674. [PubMed: 19461840]
31. Emsley P, Cowtan K. Coot: model-building tools for molecular graphics. Acta Crystallogr D Biol Crystallogr. 2004; 60:2126–2132. [PubMed: 15572765]
32. Murshudov GN, Vagin AA, Dodson EJ. Refinement of Macromolecular Structures by the Maximum-Likelihood Method. Acta Crystallogr D Biol Crystallogr. 1997; 53:240–255. [PubMed: 15299926]

33. Delano, W. The PyMol Users Manual. California: DeLano Scientific, San Carlos; 2002.
34. Sawaya MR, Sambashivan S, Nelson R, Ivanova MI, Sievers SA, Apostol MI, Thompson MJ, Balbirnie M, Wiltzius JJW, McFarlane HT, Madsen AØ, Riekel C, Eisenberg D. Atomic structures of amyloid cross-beta spines reveal varied steric zippers. Nature. 2007; 447:453–457. [PubMed: 17468747]
35. Apostol MI, Sawaya MR, Cascio D, Eisenberg D. Crystallographic studies of PrP segments suggest how structural changes encoded by polymorphism at residue 129 modulate susceptibility to human prion disease. J Biol Chem. 2010
36. Kaski D, Mead S, Hyare H, Cooper S, Jampana R, Overell J, Knight R, Collinge J, Rudge P. Variant CJD in an individual heterozygous for PRNP codon 129. Lancet. 2009; 374:2128. [PubMed: 20109837]
37. Ghani AC, Donnelly CA, Ferguson NM, Anderson RM. Updated projections of future vCJD deaths in the UK. BMC Infect. Dis. 2003; 3:4. [PubMed: 12716457]
38. Williams ES, Young S. Chronic wasting disease of captive mule deer: a spongiform encephalopathy. J. Wildl. Dis. 1980; 16:89–98. [PubMed: 7373730]
39. Williams ES, Young S. Spongiform encephalopathy of Rocky Mountain elk. J. Wildl. Dis. 1982; 18:465–471. [PubMed: 7154220]
40. Miller MW, Williams ES. Prion disease: horizontal prion transmission in mule deer. Nature. 2003; 425:35–36. [PubMed: 12955129]
41. Kong Q, Huang S, Zou W, Vanegas D, Wang M, Wu D, Yuan J, Zheng M, Bai H, Deng H, Chen K, Jenny AL, O'Rourke K, Belay ED, Schonberger LB, Petersen RB, Sy M, Chen SG, Gambetti P. Chronic Wasting Disease of Elk: Transmissibility to Humans Examined by Transgenic Mouse Models. J. Neurosci. 2005; 25:7944–7949. [PubMed: 16135751]
42. Browning SR, Mason GL, Seward T, Green M, Eliason GAJ, Mathiason C, Miller MW, Williams ES, Hoover E, Telling GC. Transmission of Prions from Mule Deer and Elk with Chronic Wasting Disease to Transgenic Mice Expressing Cervid PrP. J. Virol. 2004; 78:13345–13350. [PubMed: 15542685]
43. Gossert AD, Bonjour S, Lysek DA, Fiorito F, Wüthrich K. Prion protein NMR structures of elk and of mouse/elk hybrids. Proceedings of the National Academy of Sciences of the United States of America. 2005; 102:646–650. [PubMed: 15647363]
44. Sigurdson CJ, Nilsson KPR, Hornemann S, Heikenwalder M, Manco G, Schwarz P, Ott D, Rülicke T, Liberski PP, Julius C, Falsig J, Stitz L, Wüthrich K, Aguzzi A. De novo generation of a transmissible spongiform encephalopathy by mouse transgenesis. Proceedings of the National Academy of Sciences. 2009; 106:304–309.
45. Sigurdson CJ, Nilsson KPR, Hornemann S, Manco G, Fernández-Borges N, Schwarz P, Castilla J, Wüthrich K, Aguzzi A. A molecular switch controls interspecies prion disease transmission in mice. J. Clin. Invest. 2010; 120:2590–2599. [PubMed: 20551516]
46. Nelson R, Sawaya MR, Balbirnie M, Madsen AØ, Riekel C, Grothe R, Eisenberg D. Structure of the cross-beta spine of amyloid-like fibrils. Nature. 2005; 435:773–778. [PubMed: 15944695]
47. Gibbs CJ, Gajdusek DC. Experimental Subacute Spongiform Virus Encephalopathies in Primates and Other Laboratory Animals. Science. 1973; 182:67–68. [PubMed: 4199733]

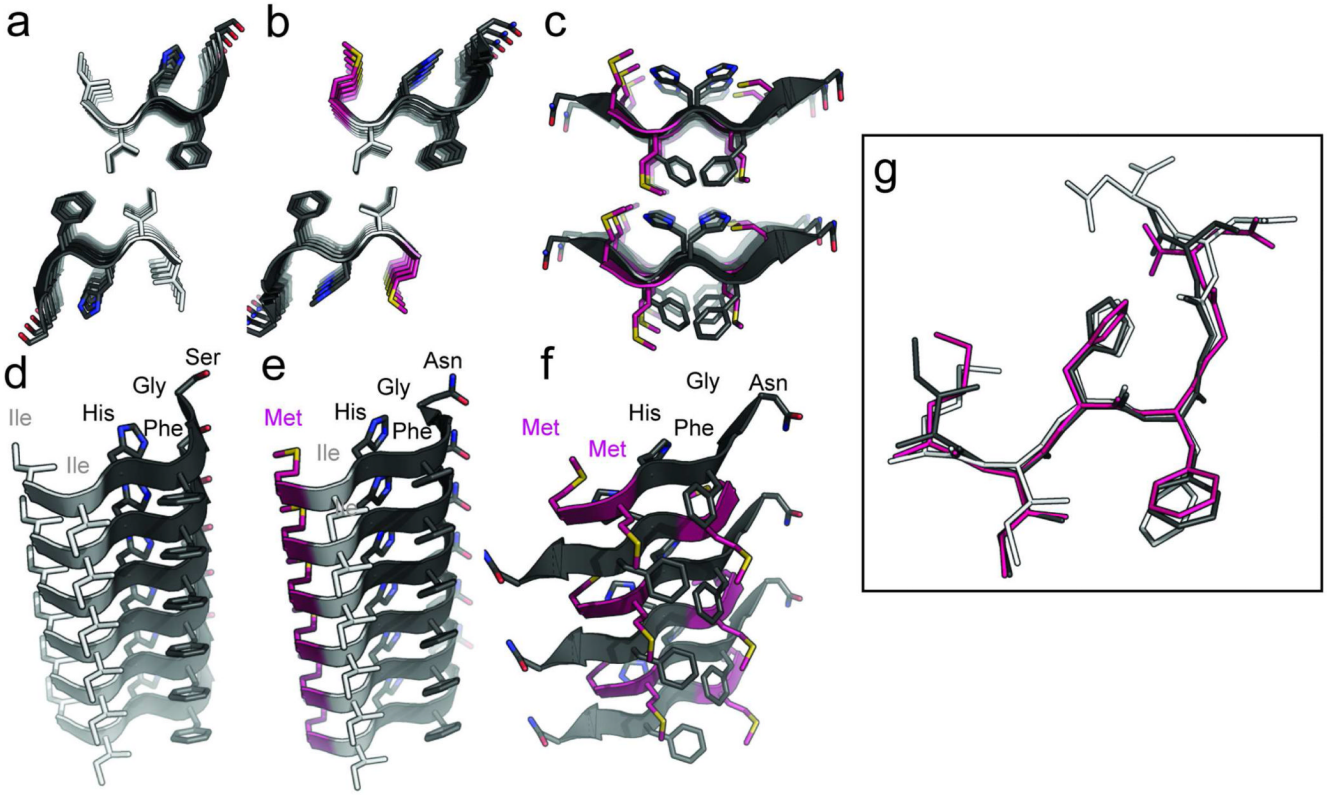

Figure 1.

Atomic structures from X-ray crystallography of steric zippers formed by the transmission-determining segment of human, mouse, and hamster PrP. The steric zippers of human (A), mouse (B), and hamster (C) segments 138–143 (using human numbering) are illustrated as cartoon representations showing sheet-to-sheet interactions. Side chains are drawn as stick representations, with carbon atoms in isoleucine residues highlighted in white, methionines in magenta, and the remaining residues in dark grey. In the side chains, nitrogen atoms are colored in blue, oxygen in dark red and sulfur in yellow. The bottom panels (D–F) show a view along the hydrogen bonding axis (length of the page) of one isolated sheet showing the stacking of β-strands. By comparing panels A and B it can be seen the two structures of human and mouse segments and interfaces are nearly identical. (G) The alignment of six-residue Hum138–143 (dark grey), six-reside Mus137–142 (magenta), and seven-residue Mus137–143 (white) have similar conformations with the characteristic kink at Gly142. A r.m.s.d of 0.53 Å was calculated between main-chain atoms of the human and mouse segments showing a great similarity across the aligned six residues. By contrast the r.m.s.d between the hamster/mouse and hamster/human structures is 3.427 Å and 3.169 Å, respectively.

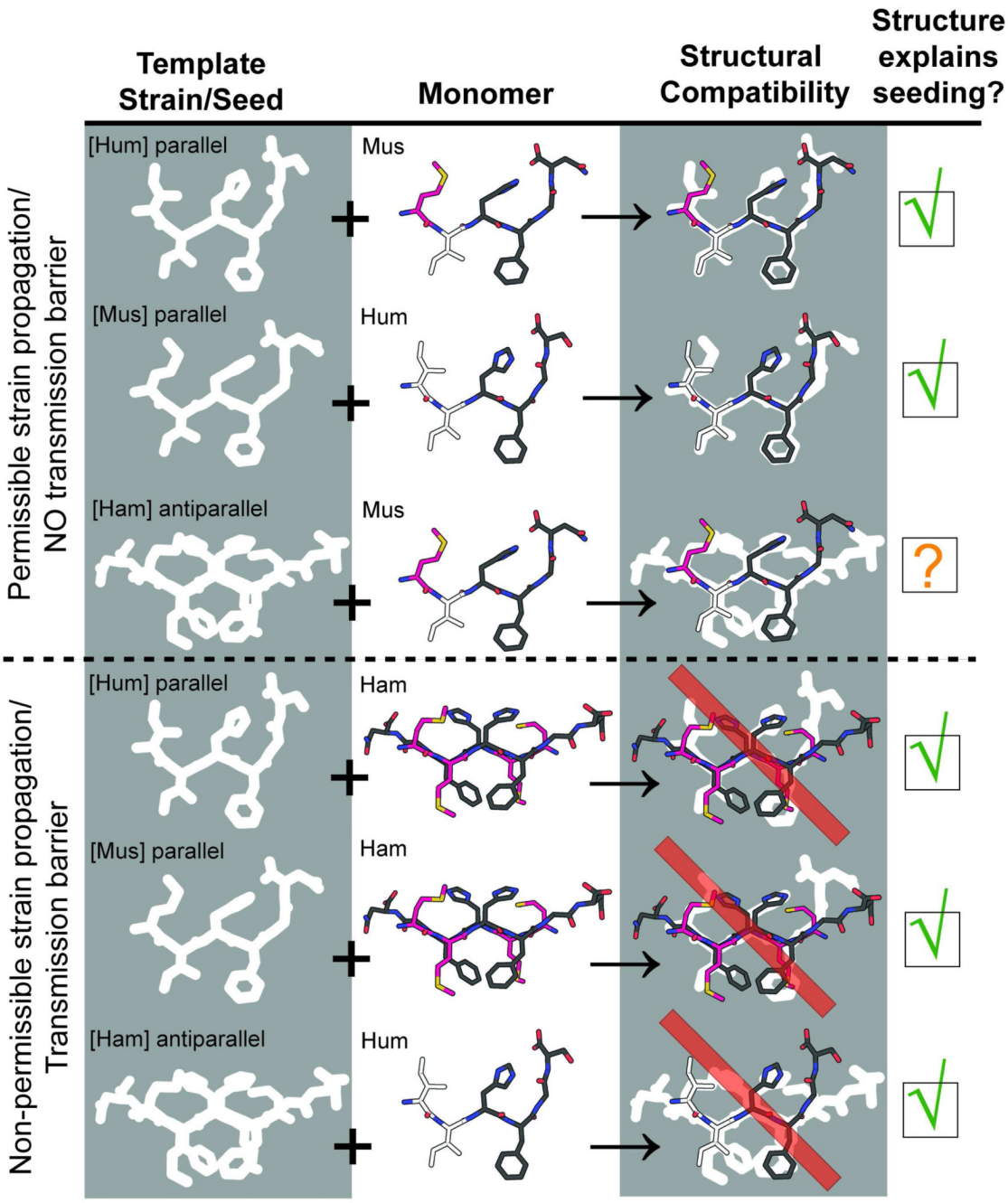

Figure 2.

Diagram analogizing the structural aspects of permissible strain propagation and transmission barriers with fitting a square-peg-in-a-round-hole. The left column represents template strains or seeds as a mold, the middle column represents monomers as sticks. To have successful seeding, the sticks have to fit in the mold. The right column shows the quality of the fit. The fourth column shows how this rationalization of structural fit matches the data presented by Vanik et al. and Jones et al. and summarized in Table 1 for the species dependent seeding of PrP23-144 (25,34).

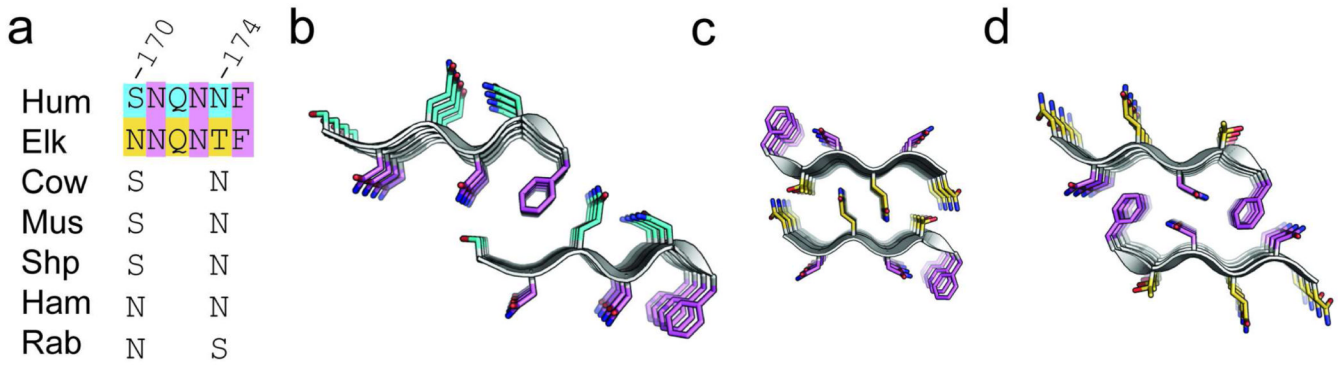

Figure 3.

(A) The sequence alignment of the region 170–175 (using human numbering) of human (Hum), elk, hamster (Ham), bovine (Cow), mouse (Mus), sheep (Shp), and rabbit (Rab) PrP. Residues corresponding to positions 170 and 174 using human numbering have species variation, however only the elk prion has both an Asn at residue 170 and Thr at residue 174. Purple highlights the xNxNxF motif common for all species, while cyan highlights the human specific residues and yellow highlights the elk specific residues. These colors are continued in the stick representations of side chains in the human segment 170–175 (B) pdb code 3fva, and both interfaces of the homologous elk segment (C and D) pdb code 2ol9. (21,33) The peptide backbone is depicted as a cartoon in white. In all the representations the hydrogen bonding axis of the beta-sheets is perpendicular to the plane of the page to point out the packing of side chains within the steric zipper interfaces.

Table 1

Strain dependent seeding of prion amyloid

Amyloid Seed	prion monomer Hum	Mus	Ham	Fibril Morphology	Sequence
[Hum]	+	+	−	Twisted	. . . I I H F G S D
[Mus]	+	+	−	Twisted	. . . M I H F G N D
[Ham]	−	+	+	Smooth	. . . M M H F G N D

This table, adapted from Jones *et al.* (26), shows that preformed amyloid of human [Hum], mouse [Mus] or hamster [Ham] PrP23–144 can be used as a seed (+) or fails to seed (−) the amyloid fiber formation from Hum, Mus or Ham monomeric PrP23-144. Twisted and smooth morphologies of fibers as examined by electron microscopy were also corroborated by distinct FTIR spectra suggesting the two are different strains. Furthermore, seeded fibrils take on the morphology of the seeds, in that [Ham] seeded Mus adopt a smooth characteristic different from the twisted morphology of both [Mus] and [Hum] fibers. The differences crucial for this property are the methioine and isoleucine residues corresponding to residues 138 and 139 (using human numbering). Theses residues are highlighted in magenta for methionine or white for isoleucine, while the rest of the relevant sequence of the 138–144 segments are highlighted in dark grey. This color scheme corresponds to the structures of the segments in Figure 2 and 3.

Table 2

Statistics of X-ray diffraction data collection and atomic refinement of the structures.

Crystal Segment Name	**138–143Ham**	**138–143Hum**	**137–142Mus**	**137–143Mus**
Sequence	**MMHFGN**	**IIHFGS**	**MIHFGN**	**MIHFGND**
Data Collection				
Collected at	UCLA	ESRF ID13	SLS X06SA	ESRF ID13
Spacegroup	$P2_1$	$P2_12_12$	$P2_12_12_1$	$P2_12_12_1$
Resolution (Å)	1.7	1.8	1.5	1.65
Unit cell dimensions: a,b,c (Å)	9.51, 11.78, 36.54	4.80, 27.54, 31.01	4.77, 27.28, 31.47	4.87, 30.28, 31.10
Unit cell dimensions: α,β,γ (°)	90.0, 93.0, 90.0	90.0, 90.0, 90.0	90.0, 90.0, 90.0	90.0, 90.0, 90.0
Measured reflections	9902	1674	4233	4503
Unique reflections	939	443	801	714
Overall completeness (%)	97.2	85.4	90.9	97.3
Last shell completeness (%)	88.0	67.0	68.8	88.7
Overall redundancy	10.5	3.8	5.3	6.3
Last shell redundancy	5.8	1.7	3.4	2.7
Overall R_{sym}	0.16	0.22	0.15	0.21
Last shell R_{sym}	0.15	0.40	0.45	0.21
Overall I/Sigma	11.9	5.4	7.6	8.5
Last shell I/Sigma	8.5	2.0	2.2	3.8
Last Shell (Å)	1.76-1.70	1.94-1.80	1.62-1.5	1.71-1.65
Refinement				
R_{work}	0.20	0.21	0.18	0.17
R_{free} (test set)	0.26 (14.8%)	0.22 (9.2%)	0.20 (11.6%)	0.19 (10.3%)
RMSD bond length (Å)	0.024	0.009	0.013	0.009
RMSD angle (°)	1.90	1.65	1.35	1.30
Number of peptide atoms	100	48	50	66
Number of solvent atoms	3	8	2	10
Average B factor of peptide (Å2)	20.7	15.6	6.9	9.5
Average B factor of solvent (Å2)	23.1	52.1	47.2	31.3
Pdb code	1NVE	1NVF	1NVG	1NVH

Table 3

Quantitative measure of fit between crystal structures of human, mouse, and hamster segments

	Hum138–143	**Mus137–142**	**Mus137–143**	**Ham138–143**
Hum138–143		0.53 Å	0.31 Å	1.65 Å
Mus137–142	0.76 Å		0.64 Å	1.45 Å
Mus137–143	0.75 Å	1.21 Å		1.30 Å
Ham138–143	1.94 Å	2.14 Å	1.72 Å	

This lookup tables shows a quantitative measure of fit between the crystallized segments of human mouse and hamster segments. Above the diagonal is the r.m.s.d of the alignment of main-chain atoms between respective structures. Below the diagonal is the r.m.s.d of the same alignments for main-chain and side-chain atoms.